IPPI

Polyolefins Journal, Vol. 12, No. 1 (2025)
DOI: 10.22063/poj.2025.35587.1339

ORIGINAL PAPER

# Fabrication and performance evaluation of mixed matrix membrane comprising Pebax and graphene hydroxyl in olefin/paraffin separation

Ahmed Fadhil Jumaah and Reza Abedini*

EOR and Gas Processing Research Lab., Faculty of Chemical Engineering,
Babol Noshirvani University of Technology, Babol, Iran

Received: 29 October 2024, Accepted: 8 January 2025

## ABSTRACT

Propylene is a widely used compound in various industrial applications, but its separation from propane, which is often associated with it, remains a significant challenge. Among the separation methods, membrane technology, particularly polymeric membranes, offers an attractive solution due to its relatively low cost and simplicity. In this study, hydroxyl-functionalized graphene (G─OH) nanosheets were used as an additive in a Pebax 1657 matrix. The results from Fourier Transform Infrared Spectroscopy (FTIR) revealed that the interaction between Pebax and G─OH is physical, characterized by a shift in some peaks due to hydrogen bonding. The proper dispersion of G─OH in the Pebax matrix was confirmed by Differential Scanning Calorimetry (DSC), which also showed an increase in the glass transition temperature ($T_g$), indicating the rigidity of Pebax chains in the presence of G─OH. Thermogravimetric Analysis (TGA) results demonstrated that the degradation temperatures ($T_d$) of Pebax/G─OH 1 wt.% and Pebax/G─OH 2 wt.% membranes were 335 °C and 330 °C, respectively. A comprehensive gas permeation study, including pure and mixed gas tests at feed pressures of 2, 6, and 10 bar, as well as a long-term stability test, was conducted on the membranes. Among all the MMMs, Pebax/G─OH 1.5 wt.% demonstrated the best gas separation performance, achieving a propylene permeability of 89.8 barrer and a $C_3H_6/C_3H_8$ selectivity of 9.8. Additionally, under mixed gas permeation tests (50:50 v/v of $C_3H_6$ and $C_3H_8$), this membrane exhibited a propylene permeability of 76.3 barrer and a $C_3H_6/C_3H_8$ selectivity of 8.8. Finally, the performance of the MMMs in $C_3H_6/C_3H_8$ separation was benchmarked against the Robeson upper bound curve. **Polyolefins J (2024) 12: 31-44**

**Keywords:** Polyether block amide; mixed matrix membrane; propylene/propane separation; Robeson bound.

## INTRODUCTION

The separation of propane ($C_3H_8$) and propylene ($C_3H_6$) is crucial in the petrochemical industry due to its significant economic and industrial importance. Propylene, a key feedstock for polypropylene production, must be of high purity to ensure the quality of polymers used in packaging, automotive, and medical applications. Its higher value compared to propane drives the need for efficient separation to maximize recovery and economic returns. Additionally, separating propane is essential for maintaining catalyst performance in downstream processes and reducing environmental impact by minimizing waste and emissions [1-3]. However, the separation is challenging due to the similar physical properties of propane and propylene, such as their close boiling points, making traditional cryogenic distillation energy-intensive. This has spurred the development of advanced techniques like adsorptive separation using metal-organic frameworks (MOFs), membrane technologies, and hybrid processes. With propylene demand rising globally, efficient propane/propylene

*Corresponding Author - E-mail: abedini@nit.ac.ir

CC BY NC SA

separation remains vital for ensuring a sustainable and steady supply for industrial applications [4,5].

Membrane technology offers a promising alternative and has significant advantages such as increased energy efficiency, compact and modular design, operational simplicity and cost-effectiveness. Membrane systems reduce energy consumption by avoiding phase changes and allow flexible scaling while lowering maintenance and operational complexity [7]. Advances in membrane materials improve selectivity for propylene over propane, leveraging differences in molecular size, polarity, or specific interactions with the membrane. Additionally, membranes have environmental benefits, including reduced energy consumption and the absence of solvents, aligning with sustainable industrial practices [8].

The materials used in membrane technology are inorganic and polymeric; inorganic materials in membrane application provide several advantages such as thermal stability, chemical resistance and mechanical strength but in contrast, they are expensive, low flexible with scale up problems [8, 9].

While, polymeric membranes are cost-effective and scalable with good processability [10]. These membranes suffer from lack of proper thermal and chemical resistance and the trade-off between permeability and selectivity [11]. Based on the glass transition temperature ($T_g$), polymers are divided into glassy ($T_g > T_{ambient}$) and rubbery ($T_g < T_{ambient}$); based on the literature, it can be concluded that glassy polymers naturally have better selectivity, while the permeability is the superior factor in rubbery polymers [12,13].

The combination of glassy and rubbery polymers can result in multi-block polymers with modified structural and performative properties in gas separation. Poly(ether-block-amide) which is known as Pebax, is a block copolymer with polyethylene oxide (PE) as soft segment and polyamide (PA) as rigid segment. The change in the type of PE and PA segments determines the grade of Pebax and consequently its properties [14]. In the Pebax structure, there are some polar functional groups such as hydroxyl, carboxyl and amino which can interact with a special gas species [15, 16]. Nevertheless, Pebax by itself cannot overcome the limitations of polymeric membranes.

However, challenges remain such as limited stability under industrial conditions, plasticization, and the trade-off between selectivity and permeability in polymeric membrane. In the case of advanced materials, such as mixed matrix membranes, research is underway aimed at addressing these challenges and fully understanding the potential of membrane technology for propane/propylene separation [17,18].

A mixed-matrix membrane (MMM) is a type of composite membrane that combines the properties of two different materials: a polymeric matrix and an inorganic filler. This hybrid structure is designed to improve the performance of traditional polymeric membranes by integrating the superior separation capabilities of inorganic materials while retaining the processability and mechanical properties of polymers [19].

A wide range of fillers was applied into a polymeric membrane to fabricate MMMs and can be classified in metal oxides ($TiO_2$, $Al_2O_3$, etc.) [20, 21], metallic ions (Cu, Ag, etc.) [22, 23], metal-organic frameworks (MOFs) (MILs, ZIFs, etc.) [24, 25], silica ($SiO_2$) [26], and carbon-based fillers (carbon nanotubes, graphene, etc.) [27, 28]. According to the diversity of filler materials, it is very important to choose a group of compatible materials for preparing these membranes. Lack of compatibility may cause several issues like interfacial defects, filler aggregation, phase separation and plasticization exacerbation, which generally impair the performance of MMMs [29].

To resolve these abnormality, a simple and useful way is surface functionalization of fillers. This method involves the addition of various functional groups (hydroxyl (—OH), carboxyl (—COOH), amine (—$NH_2$)) to the surface of the filler. Functionalization can improve the gas separation properties of MMMs through the interaction between the added functional group and $C_3H_6$ [30, 31].

In the following, some reported literature that is relevant to the purpose of this research is briefly explained. A wide variety of polymers and fillers were used to prepare modified membranes for $C_3H_6/C_3H_8$ separation.

For example, Davoodi et al. 2016 used Matrimid, a well-known glassy polymer, as the base polymer and added silica to improve its performance in $C_3H_6/C_3H_8$ separation. The result showed that the $C_3H_6$ permeability was improved from 0.12 to 0.18 barrer and $C_3H_6/C_3H_8$ selectivity was increased from 9.05 to 18.03 [32].

In another study, Sun et al. (2015) incorporated nano-porous graphene in ethyl cellulose (EC) matrix. The modified membrane containing 0.57 wt.% of nano-porous graphene showed the $C_3H_6/C_3H_8$ selectivity of 11.9 which was improved by 279 % in comparison with pure EC membrane [33].

Kim and Hong (2014) used ZIF-8 as filler for modification of Pebax 1657 membrane performance

in $C_3H_6/C_3H_8$ separation. They concluded that, the optimum loading of ZIF-8 is 7 wt.%, which could enhance $C_3H_6$ permeability form 114 barrer to 382 barrer and the $C_3H_6/C_3H_8$ selectivity from 2.4 to 3.76 at 25°C and 2 bar [34].

Najafi et al. (2020) used reduced graphene oxide (rGO) nanosheets to enhance the olefin/paraffin separation properties of polysulfone (PSF) membranes. The results showed that the MMM with 1 wt.% of rGO, increased the $C_3H_6$ permeability by 193% and $C_3H_6/C_3H_8$ selectivity by 18 % [35].

Kheirtalab et al. (2020) added graphene oxide (GO) nanoparticles to polyvinyl alcohol (PVA)-modified Pebax 1657 matrix and investigated the performance of the prepared membranes in $CO_2/CH_4$ separation. Pebax/PVA (10 wt.%)/GO (6 wt.%) was the best MMM for this purpose with $CO_2$ permeability of 236.48 barrer and $CO_2/CH_4$ selectivity of 33.63 [13].

In this study, Pebax®1657, a block co-polymer with 60% polyethylene oxide and 40% polyamide was used for preparing Pebax/graphene hydroxyl mixed matrix membrane. The hydroxyl group not only can improve the compatibility of graphene and Pebax, but also, can be effective for the permeation of $C_3H_6$ through the membrane and enhance the $C_3H_6/C_3H_8$ selectivity. All of the prepared membranes were chemically and thermally characterized and the performance of them in $C_3H_6/C_3H_8$ separation was investigated by gas permeability tests.

## EXPERIMENTAL

### Materials

Pebax 1657, the main polymeric matrix, was purchased from Arkema (France). Ethanol, with the purity of 99.9% was supplied by Merck (Germany) and used as the solvent for Pebax 1657. Hydroxyl functionalized graphene nanosheets (purity: 99.5%, diameter: 1-20μm, thickness: <40 nm, specific surface area: >150$m^2/g$, density: 1.9-2.2 $g/cm^3$) were bought form VCN Material (Iran) and applied as the additive of MMMs.

### Membrane preparation

To fabricate the MMMs, a calculated amount of Pebax 1657 was gradually dissolved in a (70/30 wt./wt.) mixture of ethanol and water at 60°C on a magnetic stirrer to form a 5 wt.% solution of polymer. After 4 h, when the dissolution of the Pebax granules was complete, G─OH nanosheets were added to the solution and stirred for 1 h to form a relatively dispersed suspension. Then, the mixture was sonicated at 60°C for 30 min and a totally uniform mixture was obtained. The mixture was casted in a Petri dish and left at room temperature for 24 h. Eventually the Petri dish was putted in an oven with temperature of 50°C for 24 h to remove the remained solvents and achieve the final MMM.

### Characterization and performance evaluation of membranes

*Field emission scanning electron microscopy (FESEM)*

To observe the morphology of pure Pebax and mixed matrix membranes accurately, the FESEM analysis was conducted using a TESCAN MIRA3 instrument. This is an electron transportation-based microscopy which need the sample to be conductive. So, the samples were coated with a thin layer of gold (~2-5 nm).

*Fourier Transform Infrared (FTIR) spectroscopy*

The functional groups of each component must be observed to confirm their structure and provide information about intermolecular interactions in MMMs. In FTIR analysis, the amount of infrared radiation passing through the sample was detected and displayed as a spectrum. To do this, a Frontier model of Perkin Elmer spectrophotometer was used in the wavenumber range of 400-4000 $cm^{-1}$.

*Differential Scanning Calorimetry (DSC)*

This analysis was used to determine the melting points, glass transition temperature and the degree of crystallinity of the prepared membranes. In this way, a sample was placed in the box and the changes in the heat capacity of the sample relative to the reference sample were recorded. Plotting heat flow against temperature yielded the DSC curve. A F200 Model device of Netzsch was used for this analysis in the range of -75 to 225°C with a heating rate of 10°C/min.

*Dynamic mechanical thermal analysis (DMTA)*

To evaluate the mechanical behavior of the fabricated membranes versus the temperature, this analysis was conducted in the temperature range of -75 to 50°C. Through this analysis, a prepared sample placed in the Pyris Diamond instrument under a small oscillating while the temperature gradually varied. The device measured the response of the sample, and the result was reported as a plot of tan(δ) versus the temperature.

*Mechanical properties*

The effect of incorporating fillers into a polymer

matrix on the strength of the membrane was evaluated using stress-strain tests conducted on a Zwick Roell instrument. Samples, each measuring 20 mm in length, were tested twice at a speed of 10 mm/min.

*Thermogravimetric Analysis (TGA)*

This analysis was used to evaluate the thermal stability of the prepared membranes and G─OH nanosheets. For this purpose, a certain amount of sample was placed in the box and its weight changes were plotted with increasing temperature. The device used was the STA1500 model from the Laboratory Exchange Company, which was used in a temperature range of 25 to 800°C at a heating rate of 10°C/min.

*Gas permeation measurement*

A constant volume setup was used to measure the single gas permeability through the pure and mixed matrix membranes. In this setup, a gas is fed to the membrane cell whose temperature is defined and stored in a downstream vessel. The instantaneous pressure of the container was measured by a precise sensor and, after processing, the pressure was plotted against time. The resulting graph was used to calculate the permeability and diffusivity coefficient by Equations (1) and (2), respectively.

$$P = \frac{273.15\times10^{10}VL}{760AT\left[\frac{(p_0\times76)}{14.7}\right]}\left(\frac{dp}{dt}\right) \quad (1)$$

$$D = \frac{L^2}{6\theta} \quad (2)$$

In these equations, $V$ is the constant volume of downstream vessel in $cm^3$, $L$ is the membrane's thickness (cm), $A$ is the effective area of membrane ($cm^2$), $T$ is the operating temperature (K), $p_0$ is the feed gas pressure (atm), dp/dt is the vessel's pressure increment at steady state condition (atm/s) and $\theta$ is the time lag (s). Figure 1 shows the permeability determination system schematically.

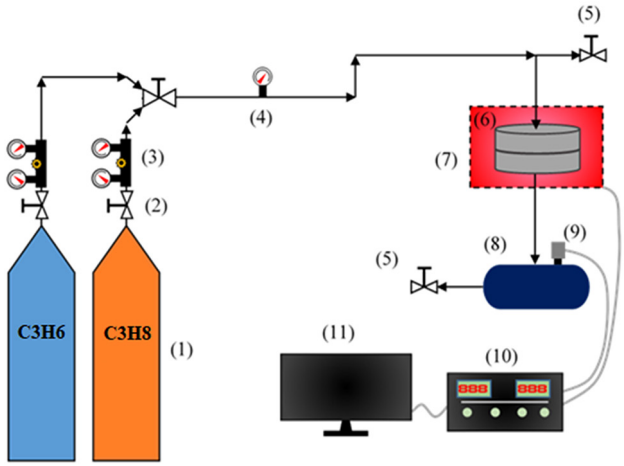



**Figure 1**. Overview of the constant volume-variable pressure system for permeability determination; (1) Gas cylinder, (2) Valve, (3) Regulator, (4) Barometer, (5) Defrost current, (6) Membrane cell, (7) Thermal element, (8) Downstream chamber, (9) Pressure sensor, (10) Pressure and temperature display and temperature element regulator, and (11) computer.

## RESULTS AND DISCUSSION

### FTIR

The FTIR spectrums of pure and mixed matrix membranes and G─OH nanosheets are represented in Figure 2. For pure Pebax, at 3295 $cm^{-1}$, there is a sharp peak which is related to H─N─C═O of PA segment. In addition, the bending vibration of N─H is indicated at 1636 $cm^{-1}$. The characteristic peak at 2863 $cm^{-1}$ is corresponded to the stretching vibration of ─$CH^3$; while, the C═O, C─O─C, and ─OH stretching vibration has appeared at 1728, 1092, and 842 $cm^{-1}$, respectively [36, 37].

The G─OH spectrum shows a broad peak at 3420 $cm^{-1}$ which is attributed to the ─OH functional group. The peak at 1374 $cm^{-1}$ is assigned to the bending vibration of C─O─H. This is the key indicator of G─OH that is reported in the literatures [38,39].

In Pebax/G─OH (0.5-2 wt.%), all Pebax and G─OH related peaks can be observed and it shows that the main intermolecular interaction is the hydrogen bond. The location of the ─OH stretching peak slightly changed due to this interaction. For example, the ─OH stretching peak shifted from 842 $cm^{-1}$ in pure Pebax to 836 $cm^{-1}$ in the Pebax/G─OH 2 wt.% spectra. Figure 3 illustrates the intermolecular interaction that could exist in the membrane structure.

### FESEM

In Figure 4, the surface and cross-sectional FESEM images of pure Pebax and Pebax/G-OH membranes are shown. For pure Pebax membrane, a uniform surface without any impurity and defect can be observed. Also, its cross-sectional image showed a uniform and dense morphology, indicating the suitability of the preparation method.

By adding G-OH nanosheets into the Pebax matrix, some white objects can be seen in the surface image,

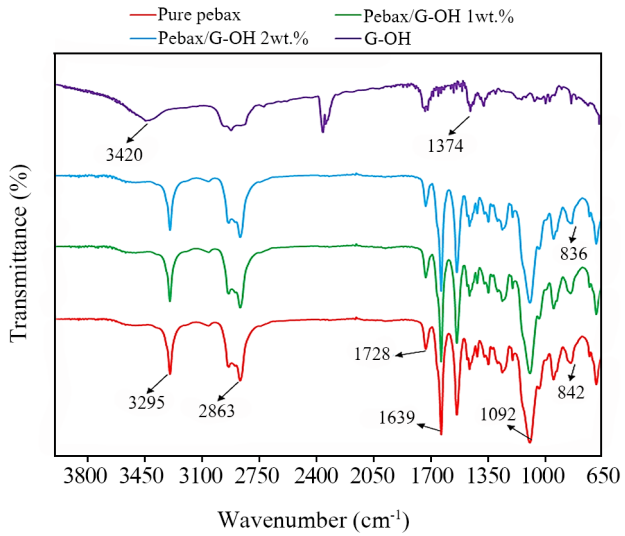



**Figure 2**. FTIR spectrums of G—OH and the prepared membranes.

which are increasing with the loading of G-OH; these are G-OH nanosheets and are obviously not properly stacked and dispersed. In cross-sectional images of MMMs, it can be seen the G-OH that nanosheets are embedded in the Pebax matrix and appear as wrinkled/ crumpled structures.

These images show that the G-OH nanoparticles are placed between Pebax chains and in this way can influence on the gas transport properties of Pebax membrane and its mechanical strength. One of the key parameters in gas permeation measurement is the overall thickness which is in the range of 30-40 μm for prepared membranes.

## DSC

To evaluate the melting point ($T_m$) and $T_g$ as the most important thermal properties of membranes and also the crystallinity of them, DSC analysis was conducted and the results are observable in Figure 5. According to this figure, there are two endothermic peaks in the curve of each membrane which are related to PE and PA segments of Pebax. As reported in Table 1, the Tm values for all prepared membranes are approximately unchanged and it says that the membranes have uniform structure without drastic changes in their crystallinity.

The $T_g$ values of the membranes, as listed in Table 1, increased with the loading of G—OH nanosheets. Its value is -52.1°C for pure Pebax and gained to -42.3°C in Pebax/G—OH 2 wt.% MMM. This can be related to the formation of hydrogen bond between the OH groups of G—OH and the carboxyl, amine and ether of Pebax, which was mentioned in detail in the FTIR section. As the G—OH loading increases, graphene sheets are placed in the Pebax matrix, stiffening its chains and thus increasing the $T_g$.

The crystallinity degrees of each membrane are also attainable from DSC curves and the values are represented in Table 1. The total crystallinity is a function of the crystallinity of the PE and PA segments of Pebax and can be described as follows:

$$X_{C\,total} = 0.6X_{C_{PE}} + 0.4X_{C_{PA}} \quad (3)$$

The $X_C$ values of PA and PE were obtained from equation 4:

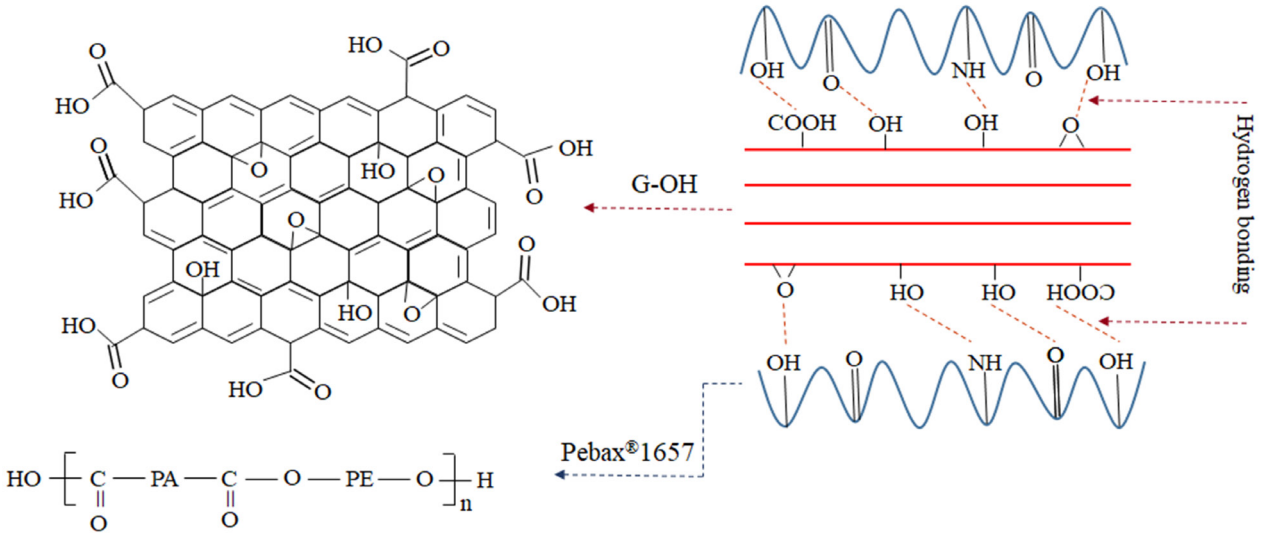



**Figure 3**. Schematic representation of possible intermolecular interaction within the mixed matrix membrane.

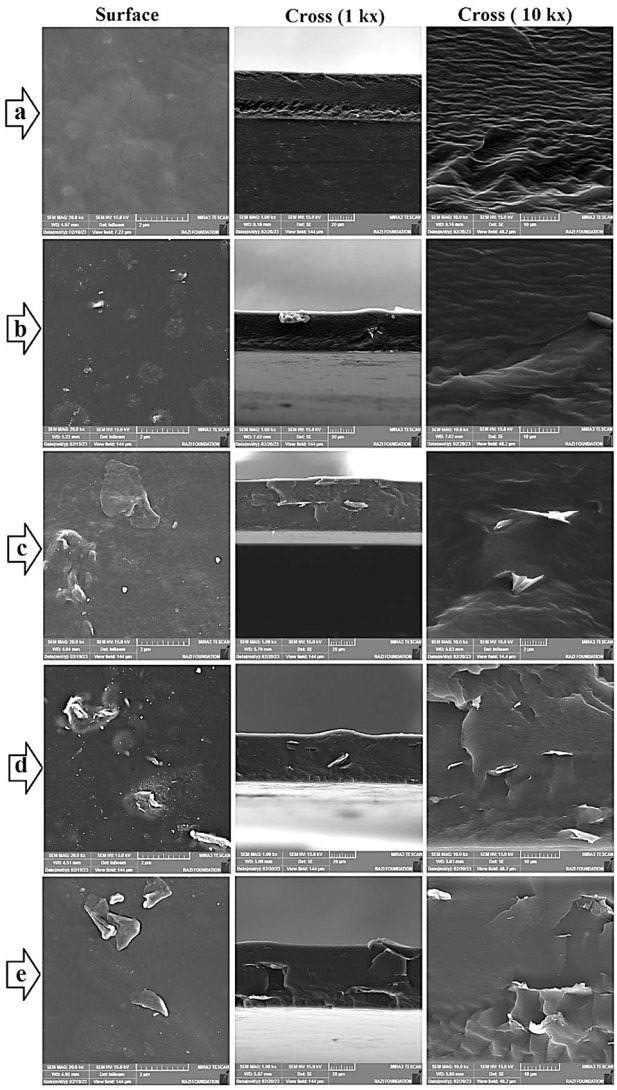



**Figure 4**. FESEM images of pure and mixed matrix membranes; a) Pure Pebax, b) Pebax/G–OH 0.5 wt.%, c) Pebax/G–OH 1 wt.%, d) Pebax/G–OH 1.5 wt.%, and e) Pebax/G–OH 2 wt.%.

$$X_c(\%) = \frac{\Delta H_m}{\Delta H_m^0} \times 100 \quad (4)$$

where $\Delta H_m$ is the required heat for melting the crystals and can be obtained from the under melting peak area and $\Delta H_m^0$ is the melting enthalpy at 100% crystalline state. This value for PE and PA parts of Pebax 1657 are 166.4 J/g and 230 J/g, respectively [44].

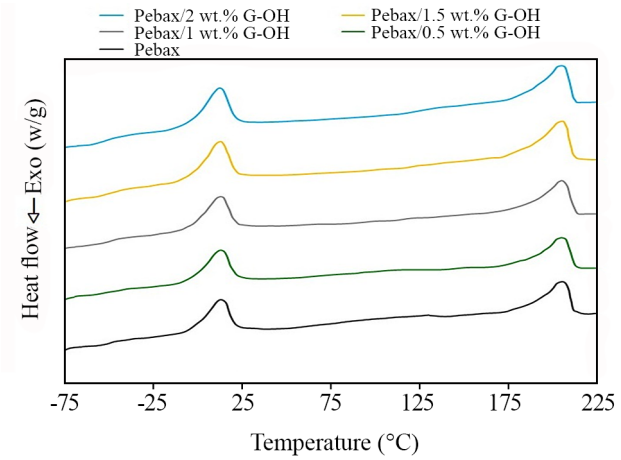



**Figure 5**. DSC curves of the prepared membranes.

According to Table 1, the trend of crystallinity changes is descending and reduced form 22.6% in pure Pebax membrane to 20.9% in Pebax/G–OH 2 wt.% MMM. The G–OH nanosheets when added to the matrix of Pebax, can disrupt the crystalline order, hindering the formation of well-defined crystals and reducing the total degree of crystallinity. Also, the hydroxyl groups of the nanosheets interact with the polar regions of Pebax chain and restrict the crystal formation [45].

## TGA

The TGA thermograms of G–OH, pure Pebax membrane and the prepared MMMs are depicted in Figure 6. For pure Pebax, about 5% weight loss occurred at 50 to 70°C and can be related to the moisture and remained solvent removal. Then main degradation of Pebax is observable at 340°C which leads to 92% weight loss of Pebax sample which is consistent with other reports [40,41].

In the case of G–OH, there are several degradation steps; first, below 100°C, the physically adsorbed water was evaporated. Then, between 100 and 200°C, the chemically bonded water with the hydroxyl groups of G–OH was removed. Also, the hydroxyl, as labile oxygen-containing functional group, can

**Table 1**. The results of DSC analysis.

| Membrane | $T_g$ (°C) | $T_{m,PE}$ (°C) | $T_{m,PA}$(°C) | $X_{C,PE}$ (%) | $X_{C,PA}$ (%) | $X_{C,Total}$ (%) |
|---|---|---|---|---|---|---|
| **Pebax** | -52.1 | 16.3 | 207.2 | 16.2 | 32.4 | 22.6 |
| **Pebax/0.5 wt.%G-OH** | -49.7 | 16.8 | 207.6 | 15.9 | 31.7 | 22.2 |
| **Pebax/1 wt.%G-OH** | -47.2 | 17.1 | 208.1 | 15.5 | 30.9 | 21.6 |
| **Pebax/1.5 wt.%G-OH** | -44.1 | 16.9 | 208.3 | 15.3 | 30.4 | 21.3 |
| **Pebax/2 wt.%G-OH** | -42.3 | 17.2 | 208.8 | 14.8 | 30.1 | 20.9 |

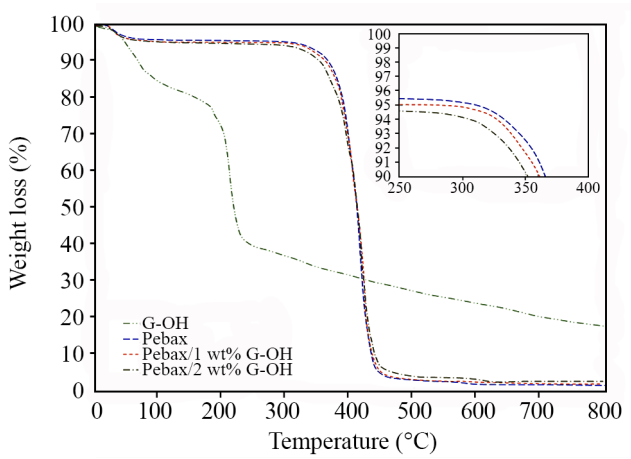



**Figure 6**. TGA curves of G—OH, pure Pebax and MMMs.

decompose and release water vapor at this range of temperature. Along 200 to 230°C, the hydroxyl groups decomposition was completed and lead to 60% weight loss. Over 230°C, the C—C bonds break down and by removing some lighter and smaller carbon particles, as gaseous compounds in some cases, the weight lost with a gentle slope [42,43].

In the Pebax/G—OH 1 and 2 wt.% MMMs, the main degradation temperature, as can be seen in magnified Figure 4, decreased by about 5 and 10°C, respectively, and can be corresponded to the lower degradation temperature of G—OH.

## Mechanical properties

The effect of zeolite loading on the tensile properties of Pebax membranes is illustrated in Figure 7. The mechanical strength of Pebax membranes is primarily attributed to the PA segments, while the PEO segments provide ductility. Consequently, the interaction of fillers with these segments significantly influences the plasticity, tensile strength, and elasticity of the membrane.

The tensile strength and elongation of the membranes exhibit opposing trends with increasing G–OH content. The elongation reduction is minimal for Pebax/0.5wt.% G–OH (from 504.4% to 489.2%) compared to neat Pebax, nonetheless becomes significant at higher loadings, with values of 435.6% and 416.8% for Pebax containing 1.5 and 2 wt.% of G–OH, respectively. This reduction can be attributed to the disruption of polymer chains by G–OH nanoparticles, as the rigid G–OH crystals replace flexible polymer chains, reducing membrane flexibility. Additionally, agglomeration of particles at higher loadings may contribute to this effect.

The tensile strength, representing sample stiffness, decreases in Pebax/0.5 wt.% G–OH and Pebax/1.5 wt.% G–OH, dropping from 234.6 MPa for the neat membrane to 221.3 MPa and 186.7 MPa, respectively. However, a sharp reduction to126.8 MPa is observed in Pebax/2 wt.% G–OH, likely due to particle clustering in the membrane.

In conclusion, the incorporation of G–OH zeolites into the polymer matrix tighten the membrane structure, increasing its rigidity and consequently reducing its tensile strength.

## DMTA

The result of this analysis is depicted in Figure 3 as a plot of damping factor (tan(δ)) versus temperature. Damping factor represents the ratio of loss modulus (E") to storage modulus (E') and it can be useful for understanding the mechanical behavior of the membrane against temperature. The peak of the curve in Figure 8 is related to the $T_g$ of the membranes. It

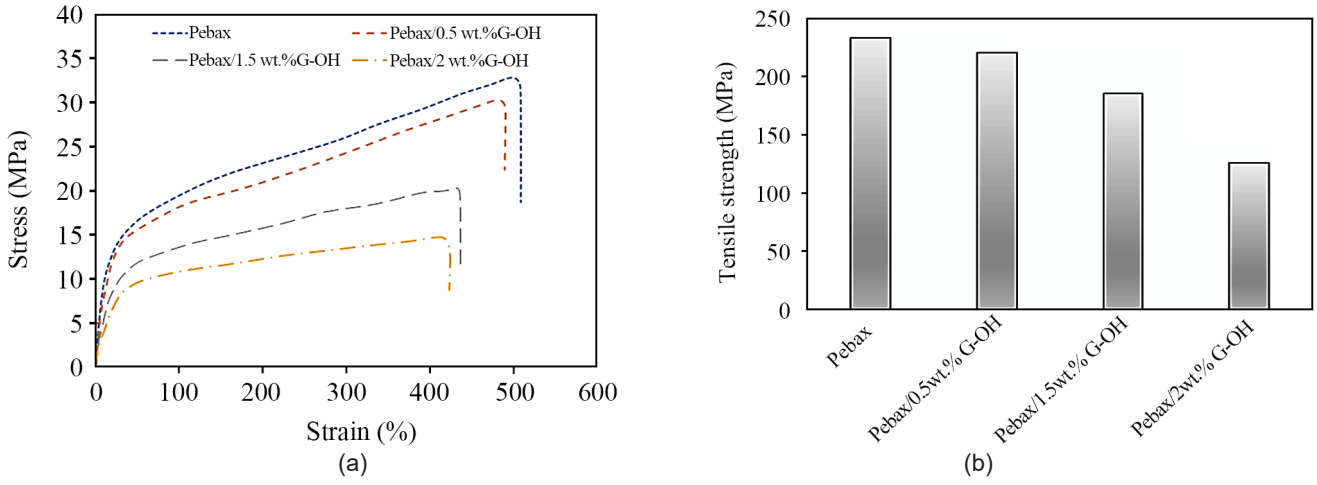



**Figure 7**. (a) Tensile stress-strain curves and (b) tensile strength of neat Pebax and some selected MMMs.

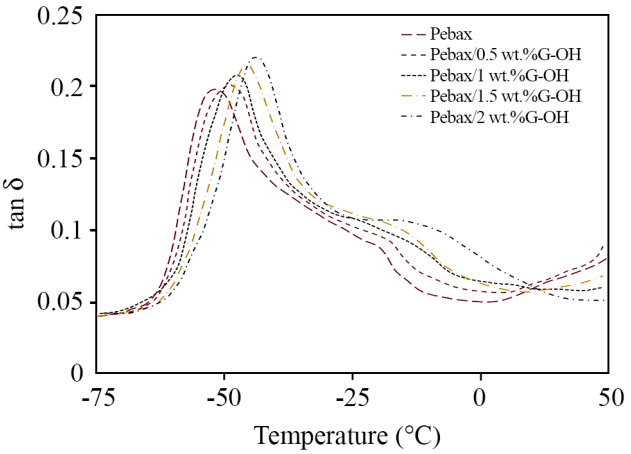



**Figure 8**. DMTA curves of prepared membranes.

is evident that the increase in G─OH loading causes the increase in $T_g$ and its value for pure Pebax, and 0.5, 1, 1.5, and 2 wt.% G─OH MMMs is -45.4, -41.5, -40.2, -37.9, and -37.5°C, respectively. As discussed in the DSC section, the formation of hydrogen bond between the Pebax and G─OH is the reason of the $T_g$ gaining. The mobility of the chains is limited by the arrangement of graphene nanosheets in chains, and consequently, the force applied to the MMM samples is mainly dedicated to overcoming this limitation.

## Gas permeation results

To evaluate the separation performance of the prepared membranes, the gas permeation test was conducted at a temperature of 30°C and 2, 6 and 10 bar of pressure. Before interpreting the results of gas permeation tests, it is necessary to review the physical properties of $C_3H_6$ and $C_3H_8$ as listed in Table 2. By this knowledge, the effect of solubility and diffusivity, which are directly involved in permeability value, can be separately investigated.

### *Effect of G─OH content*

The gas permeation results of pure Pebax and Pebax/G─OH membranes, at 30°C of temperature and 2 bar of pressure, are shown in Figure 9. According to Figure 9-a, the permeability of $C_3H_6$ is notably higher than that of $C_3H_8$. This difference can be explained in two general aspects; 1) the $C_3H_6$ molecule specification, and 2) the affinity of membrane to $C_3H_6$. In terms of molecular size and shape, $C_3H_6$ as an unsaturated hydrocarbon has a double bond (C=C) between two of its carbon atoms and the presence of this double bond makes it a planar molecule in comparison with $C_3H_8$. $C_3H_6$ is more polarizable and its kinetic diameter (4.68 Å) is slightly larger than $C_3H_8$ (4.3 Å).

In spite of larger size, the double bond causes a flat structure and allow $C_3H_6$ to pass through the polymer matrix more easily. As shown in Figure 1-a, the permeability of both gases is increasing with the loading of G─OH. For $C_3H_6$, the slope of permeability increment is approximately constant up to 1 wt. % loading of G─OH and after that, in Pebax/G─OH 1.5 wt.% the slope extremely gains followed by a reduction at the 2 wt.% containing G─OH nanosheets. The permeability values for pure Pebax and Pebax/G─OH (0-2) wt.% membranes are 19.54, 29.86, 37.71, 53.47, and 62.28 barrer, respectively.

This can be related to proper placement of G─OH nanosheets among Pebax chains and their good interaction with amine and carboxyl groups of Pebax as depicted in Figure 10. The hydrogen atoms of hydroxyl groups in G─OH can be attracted by oxygen atoms and nitrogen atoms of Pebax through hydrogen bonding. Also, the oxygen atoms of G─OH hydroxyls, interact with the hydrogen atoms of amino and carboxyl groups of Pebax. This proper compatibility, makes this membranes matrix selective for $C_3H_6$. At 2 wt.% loading of G─OH, the optimal chain packing started disruption and the slope of $C_3H_6$ permeability was declined. Meanwhile, a constant increasing trend was observed for the permeability of $C_3H_6$ in all membranes, and this can be attributed to less affectability of $C_3H_8$ than $C_3H_6$ from membranes morphology.

According to this explanation, the selectivity behavior of prepared membranes, as shown is Figure 9-b, can be easily described. The Pebax/G─OH 2 wt.% membrane, has the best $C_3H_6/C_3H_8$ selectivity and its value is 8.37 which is increased by 34% in comparison with pure Pebax membrane (6.22). In Figure 6-c, the effect of G─OH content on the diffusion of $C_3H_6$ and $C_3H_8$ through the membranes. As can be seen, the smaller minimum dimension of $C_3H_6$ than $C_3H_8$ [46], its planner structure and most importantly the sieving effect of graphene nanosheets, provides an ascending

**Table 2**. Physical properties of test gases [3].

| Component | Kinetic diameter (Å) | Condensability (K) | Dipole moment (D) |
|---|---|---|---|
| $C_3H_6$ | 4.68 | 225 | 0.366 |
| $C_3H_8$ | 4.3 | 231 | 0.083 |

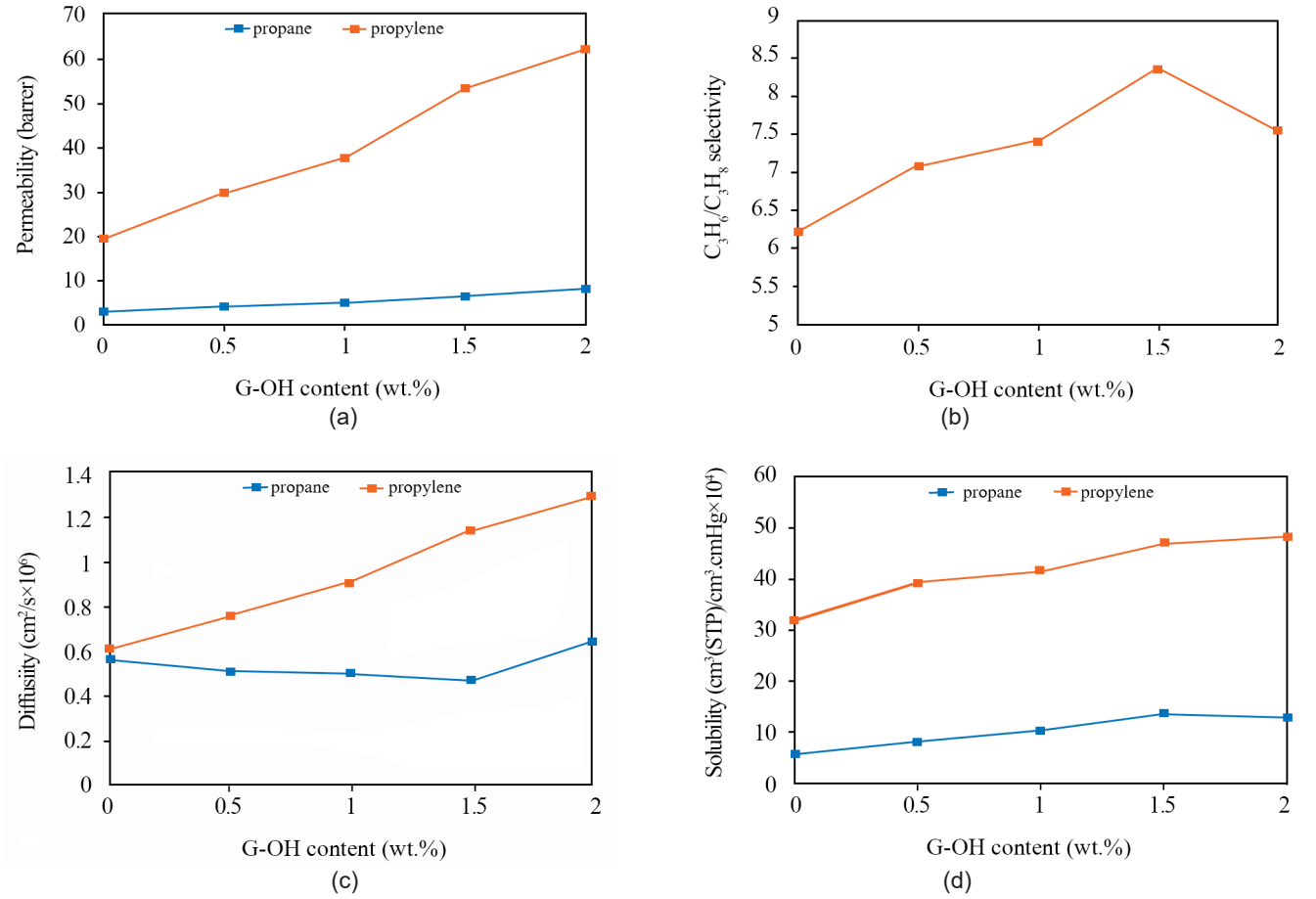



**Figure 9**. Effect of G—OH content on a) $C_3H_6$ and $C_3H_8$ permeability, b) $C_3H_6/C_3H_8$ selectivity, c) $C_3H_6$ and $C_3H_8$ diffusivity and d) $C_3H_6$ and $C_3H_8$ solubility at 2 bar and 30°C.

diffusivity trend. While, for $C_3H_8$, the diffusivity coefficient decreases up to 1.5 wt.% of G—OH because of its structural limitation and then in Pebax/G—OH 2 wt.% membrane, the diffusivity increased because of the membrane's morphological defects as discussed in FESEM section. Figure 6-d shows the solubility changes in the prepared membranes.

According to this figure, the solubility for $C_3H_6$ is higher than $C_3H_8$ due to its greater interaction with the membranes. The trend of this parameter is almost similar for $C_3H_6$ and $C_3H_8$ and can be related to the same effect of membranes on these gases. In other words, the structural features of the gases affect their solubility.

*Effect of feed pressure*

In Figure 11, the effect of feed pressure on separation parameters of pure and mixed matrix membranes is depicted. As can be seen in Figure 11-a, the permeability of both gases is increasing with feed pressure increment and it may generally cause by the driving force of gas transport across the membrane. Besides, at higher pressures, the concentration of gases increased in feed side of the membrane and it is a good opportunity for polarizable gases to interact with the membrane and absorbed by it. In the case of $C_3H_6/C_3H_8$, according to Figure 11-a, the feed pressure increment is more effective on the permeability of $C_3H_6$ due to its planer structure and its higher dipole moment value.

In Figure 11-b, the $C_3H_6/C_3H_8$ selectivity can be observed. For pure and mixed matrix membranes with G—OH content up to 1.5 wt.%, the selectivity increased by pressure because of aforementioned reason and there is no plasticization effect in these membranes; for example, in Pebax/G—OH 1.5 wt.%, the selectivity enhanced from 8.37 at 2 bar, to 9.82 at 10 bar. However, in Pebax/G—OH 2 wt.%, the selectivity decreased with increasing pressure, indicating that plasticization occurred in this membrane.

It can be related the chain compactness and irregular placement of graphene nanosheets among Pebax chains. By increasing the pressure, the interchain free spaces reduced and the permeation of gases through

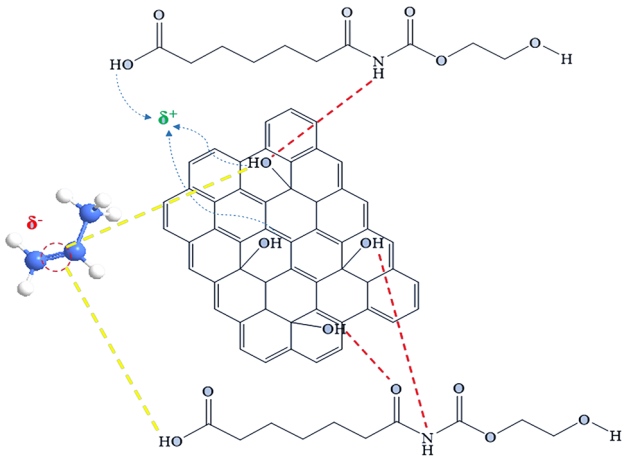



**Figure 10**. Schematic representation of propylene interaction with the MMM matrix (Red-dashed line: Hydrogen bond, Yellow-dashed line: Electrostatic bond).

the membrane disturbed. $C_3H_6$, which has more interaction with membrane and passes easier than $C_3H_8$, affected extremely and results in selectivity decreasing. In term of diffusivity (Figure 11-c), the effect of feed pressure on $C_3H_6$'s diffusion is more than $C_3H_8$'s because of $C_3H_6$'s planer structure which causes its easier transportation.

The solubility of $C_3H_6$ and $C_3H_8$ can be observed in Figure 11-d. For $C_3H_8$ in all membranes, the solubility increases with pressure and there is a small difference between its value at 6 and 10 bar for the MMMs with 1.5 and 2 wt.% of G—OH. It can be related to chain compressing of these membranes which causes the reduction of interaction chance for $C_3H_8$ molecules.

$C_3H_6$'s solubility is also increased by pressure increment for pure and 0.5 and 1 wt.% G—OH containing membranes due to proper interaction with the membranes' selective groups such as amino, carboxyl and amino. These interactions are disrupted at higher pressures because of the compressing of chine and reducing interchain selective free space.

The mixed gas permeation properties of MMM filled by 1.5 wt.% G–OH were evaluated using $C_3H_6/C_3H_8$

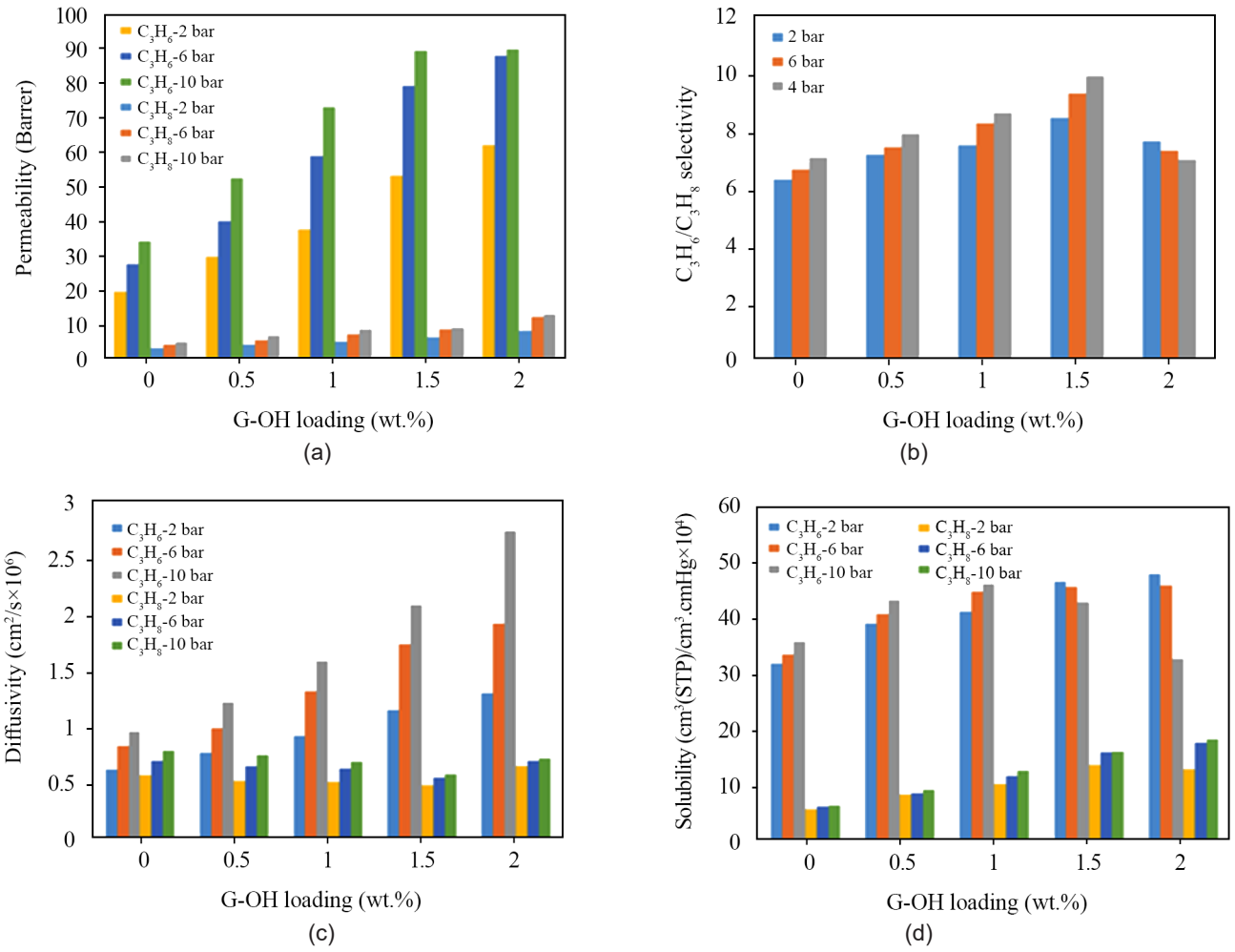



**Figure 11**. Effect of feed pressure on: a) propylene and propane permeability, b) propylene/propane selectivity, c) propylene and propane diffusivity, and d) propylene/propane solubility.

**Table 3**. Mixed gas separation performance of selected MMM compared to ideal separation.

| Membrane | Pure gas tests | | | Mixed gas tests | | |
|---|---|---|---|---|---|---|
| | Permeability (barrer) | | $C_3H_6/C_3H_8$ Ideal Selectivity | Permeability (barrer) | | $C_3H_6/C_3H_8$ Real Selectivity |
| | $C_3H_6$ | $C_3H_8$ | | $C_3H_6$ | $C_3H_8$ | |
| Pebax/1.5 wt.% G-OH | 2 bar | | | | | |
| | 53.47 | 6.38 | 8.36 | 46.95 | 6.15 | 7.63 |
| | 6 bar | | | | | |
| | 79.57 | 8.64 | 9.2 | 68.75 | 8.22 | 8.36 |
| | 10 bar | | | | | |
| | 89.85 | 9.15 | 9.8 | 76.34 | 8.66 | 8.81 |

gas mixtures at a 50:50 v/v ratio. After the gas mixtures passed through the membrane, the non-permeable flow was removed, and the composition of the permeable flow was analyzed using gas chromatography (GC). The permeability and selectivity results for the gas mixture, measured at 2, 6 and 10 bar and 30°C, are summarized in Table 3.

Comparison of these results with pure gas permeability data (Table 3) shows that, the permeability of $C_3H_6$ and the $C_3H_6/C_3H_8$ selectivity are lower in mixed gas conditions compared to pure gas conditions. This reduction is attributed to the interaction between $C_3H_6$ and $C_3H_8$ in the mixture.

The data also reveal a decrease in selectivity when $C_3H_8$ is present.

The table illustrates the effect of feed pressure on the performance of MMMs containing MOF particles for gas mixture separation. The trends in permeability and selectivity closely mirrored those observed for pure gas permeability and ideal $C_3H_6/C_3H_8$ selectivity. However, the mixed gas results consistently showed lower permeability and selectivity than the pure gas values.

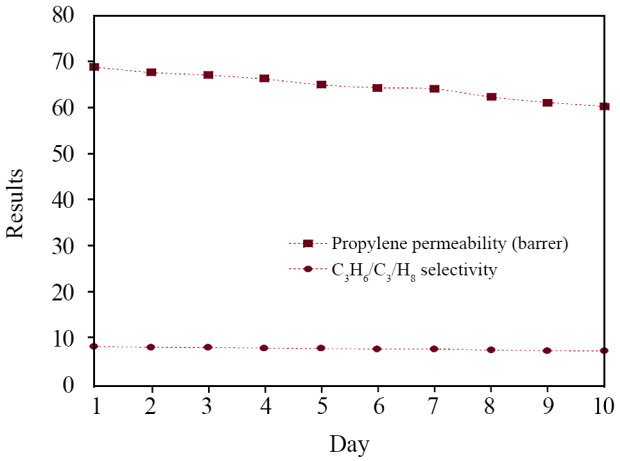



**Figure 12**. Propylene permeability and real $C_3H_6/C_3H_8$ selectivity of MMM (1.5 wt.% G–OH) versus time (day) under temperature of 30°C and pressure of 6 bar.

*Membranes performance evaluation*

The reduction in gas permeability over time, due to limited stability, is a significant challenge hindering the widespread commercial adoption of polymeric membranes. Enhancing the durability of polymeric membranes is therefore a critical priority for developing viable membrane technologies. Interactions between membrane components can mitigate physical aging and improve resistance to plasticization, thereby enhancing membrane performance. In this study, the stability of a mixed matrix membrane (MMM) containing 1.5 wt.% G–OH was evaluated under mixed gas permeation conditions for 10 days at 30 °C and 6 bar. As illustrated in Figure 12, the MMM exhibited relatively stable propylene permeability throughout the testing period, with only a modest reduction of approximately 10%.

The ability of the membranes to permit $C_3H_6$ permeability and $C_3H_6/C_3H_8$ selectivity compared to the Robeson's upper bound is illustrated in Figure 13. According to this figure, for pure and mixed matrix membranes with G─OH content up to 1.5 wt.%, the performance points approach to upper bound while for MMM with 2 wt.% of G─OH, this trend is reverse.

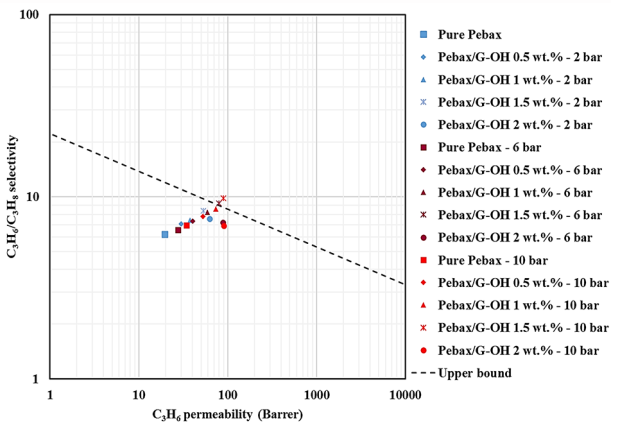



**Figure 13**. Comparison the results of this study with Robeson's upper bound.

By increasing the feed pressure and enhancing the $C_3H_6$ permeability and $C_3H_6/C_3H_8$ selectivity, the MMMs with 0.5, 1, 1.5 wt.% G─OH content showed better performance while for Pebax/G─OH 2 wt.%, the significant reduction in $C_3H_6/C_3H_8$ selectivity turned away the performance point from the upper bound. Consequently, the best performance is related to Pebax/G─OH 1.5 wt.% at 10 bar.

## CONCLUSION

In this work, a Pebax-based MMM continuing hydroxyl-functionalized graphene nanosheets was fabricated. The prepared membranes were characterized by FTIR, FESEM, DSC, TGA, and DMTA. The FTIR results showed that the intermolecular interactions are physical and there is no new functional group in the MMMs spectrums. The FESEM images confirmed the effect G─OH nanosheets on the morphology of prepared MMMs by a wrinkled pattern. In the DSC analysis, the $T_g$ of MMMs was increased by adding G─OH nanosheets to the Pebax matrix and it was related to chain rigidification of MMM in the presence of G─OH nanosheets. This trend was emphasized by DMTA curves for MMMs. Thermograms of TGA analysis for MMMs showed that the addition of G─OH nanosheets to Pebax reduces its thermal stability. The gas permeation results indicated that the Pebax/G─OH 1.5 wt.% has the best selectivity value and the optimum loading of G─OH nanosheets was 1.5 wt.% without any plasticization up to 10 bar of feed pressure. The best separation performance attained was propylene permeability of 89.85 barrer and $C_3H_6/C_3H_8$ selectivity of 9.81 at feed pressure of 10 bar. The mixed gas permeability tests also implied the 10% performance loss in Pebax/G─OH 1.5 wt.% over the 10 days long term test. The best separation performance achieved was a propylene permeability of 89.85 barrer and a $C_3H_6/C_3H_8$ selectivity of 9.81 at a feed pressure of 10 bar. The mixed gas permeability tests also indicated a 10% performance loss in Pebax/G─OH 1.5 wt.% over the 10-day long-term test.

## ACKNOWLEDGEMENTS

This work was supported by the Babol Noshirvani University of Technology under Grant BNUT/393054/2023.

## CONFLICTS OF INTEREST

No potential competing interest was reported by the authors.

## REFERENCES

1. Chen XY, Xiao A, Rodrigue D (2022) Polymer-based membranes for propylene/propane separation. Sep Purif Rev 51: 130-142
2. Bora P, Bhuyan C, Rajguru P, Hazarika S (2023) A Gemini basic ionic liquid and functionalized cellulose nanocrystal-based mixed matrix membrane for $CO_2/N_2$ separation. Chem Commun 59: 12887-12890
3. Guo M, Kanezashi M (2021) Recent progress in a membrane-based technique for propylene/propane separation. Membranes 11: 310
4. Ma X, Williams S, Wei X, Kniep J, Lin Y (2015) Propylene/propane mixture separation characteristics and stability of carbon molecular sieve membranes. Ind Eng Chem Res 54: 9824-9831
5. Bharali P, Das I, Sarmah H, Hazarika S (2023) Stripping of carbon dioxide from ethanol solution of PAMAM dendrimer using hollow Fibre membrane contactor. Heat Mass Trans 59: 299-308
6. Doosti M, Abedini R (2022) Polyethyleneglycol-modified cellulose acetate membrane for efficient olefin/paraffin separation. Energy Fuels 36: 10082-10095
7. Ren Y, Liang X, Dou H, Ye C, Guo Z, Wang J, Pan Y, Wu H, Guiver MD, Jiang Z (2020) Membrane-based olefin/paraffin separations. Adv Sci 7: 2001398
8. Bhuyan C, Bora P, Rajguru P, Hazarika S (2025) Thin film nanocomposite membrane ornamented with Z-scheme heterojunction carbon dot/NiFe–LDH for removal of organic contaminants from industrial wastewater. Sep Purif Technol 356: 129791
9. Faiz R, Li K (2012) Polymeric membranes for light olefin/paraffin separation. Desalination 287: 82-97
10. Nematollahi MH, Carvalho PJ, Coutinho JAP, Abedini R (2022) Recent progress on Pebax-based thin film nanocomposite membranes for $CO_2$ capture: The state of the art and future outlooks. Energy Fuels 36: 12367-12428

11. Nobakht D, Abedini R (2023) A new ternary Pebax®1657/maltitol/ZIF-8 mixed matrix membrane for efficient $CO_2$ separation. Process Saf Environ Prot 170: 709-719
12. Hassanzadeh H, Abedini R, Ghorbani M (2022) $CO_2$ Separation over $N_2$ and $CH_4$ light gases in sorbitol-modified poly(ether-block-amide) (Pebax 2533) membrane. Ind Eng Chem Res 61: 13669-13682
13. Kheirtalab M, Abedini R, Ghorbani M (2020) A novel ternary mixed matrix membrane comprising polyvinyl alcohol (PVA)-modified poly (ether-block-amide) (Pebax®1657)/ graphene oxide nanoparticles for $CO_2$ separation. Process Saf Environ Prot 144: 208-224
14. Kheirtalab M, Abedini R, Ghorbani M (2024) Pebax/poly(vinyl alcohol) mixed matrix membrane incorporated by amine-functionalized graphene oxide for $CO_2$ separation. J Polym Sci 62: 517-535
15. Ranjbar F, Abedini R, Ghorbani M, Ghasemi M (2022) The experimental/theoretical study over the effect of using the POP-$NH_2$ nanostructures into the membrane selective layer on the $CO_2$ permeability and selectivity. Chem Eng Res Des 187: 184-195
16. Nematollahi MH, Carvalho PJ, Coutinho JAP, Abedini R (2023) Tailoring the $CO_2$ permeation of Pebax1657/polyether imide thin film composite membrane via embedding Ag-based metal-organic framework. Chem Eng Res Des 197: 109-126
17. Kim SY, Cho Y, Kang SW (2020) Preparation and characterization of PEBAX-5513/AgBF4/ BMIMBF4 membranes for olefin/paraffin separation. Polymers 12: 1550
18. Park CH, Lee JH, Jung JP, Kim JH (2017) Mixed matrix membranes based on dual-functional MgO nanosheets for olefin/paraffin separation. J Membrane Sci 533: 48-56
19. Raouf M, Abedini R, Omidkhah M, Nezhadmoghadam E (2020) A favored $CO_2$ separation over light gases using mixed matrix membrane comprising polysulfone/polyethylene glycol and graphene hydroxyl nanoparticles. Process Saf Environ Prot 133: 394-407
20. Moghadam F, Omidkhah M, Vasheghani-Farahani E, Pedram MZ, Dorosti F (2011) The effect of $TiO_2$ nanoparticles on gas transport properties of Matrimid5218-based mixed matrix membranes. Sep Purif Technol 77: 128-136
21. Fakoori M, Azdarpour A, Abedini R, Honarvar B (2021) Effect of Cu-MOFs incorporation on gas separation of Pebax thin film nanocomposite (TFN) membrane. Korean J Chem Eng 38: 121-128
22. Bora P, Bhuyan C, Borah AR, Hazarika S (2023) Carbon nanomaterials for designing next-generation membranes and their emerging applications. Chem Commun 59: 11320-11336
23. Salestan SK, Rahimpour A, Abedini R (2021) Experimental and theoretical studies of biopolymers on the efficient $CO_2/CH_4$ separation of thin-film Pebax®1657 membrane. Chem Eng Process 163: 108366
24. Mozafari M, Abedini R, Rahimpour A (2018). Zr-MOFs-incorporated thin film nanocomposite Pebax 1657 membranes dip-coated on polymethylpentyne layer for efficient separation of $CO_2/CH_4$. J Mater Chem A 6: 12380-12392
25. Meshkat S, Kaliaguine S, Rodrigue D (2018) Mixed matrix membranes based on amine and non-amine MIL-53(Al) in Pebax® MH-1657 for $CO_2$ separation. Sep Purif Technol 200: 177-190
26. Khoshhal Salestan S, Pirzadeh K, Rahimpour A, Abedini R (2021) Poly (ether-block amide) thin-film membranes containing functionalized MIL-101 MOFs for efficient separation of $CO_2/CH_4$. J Environ Chem Eng 9: 105820
27. Pacheco MJ, Vences LJ, Moreno H, Pacheco JO, Valdivia R, Hernández C (2021) Review: Mixed-matrix membranes with CNT for $CO_2$ separation processes. Membranes 11: 457
28. Pazani F, Aroujalian A (2021) High-performance gas separation using mixed-matrix composite membranes containing graphene nanoplatelets. Polym Bull 78: 6847-6866
29. Nasir R, Mukhtar H, Man Z, Mohshim DF (2013) Material advancements in fabrication of mixed-matrix membranes. Chem Eng Technol 36: 717-727
30. Lin Z, Yuan Z, Dai Z, Shao L, Eisen MS, He X (2023) A review from material functionalization to process feasibility on advanced mixed matrix membranes for gas separations. Chem Eng J 475: 146075
31. Qin Z, Ma Y, Wei J, Guo H, Wang B, Deng J, Yi C, Li N, Yi S, Deng Y, Du W, Shen J, Jiang W, Yao L, Yang L, Dai Z (2024) Recent progress in ternary mixed matrix membranes for $CO_2$ separation. Green Energy Environ 9: 831-858
32. Davoodi S, Sadeghi M, Naghsh M, Moheb A

(2016) Olefin–paraffin separation performance of polyimide Matrimid®/silica nanocomposite membranes. RSC Adv 6: 23746-23759
33. Sun HX, Yuan BB, Li P, Wang T, Xu YY (2015) Preparation of nanoporous graphene and the application of its nanocomposite membrane in propylene/propane separation. Func Mater Lett 8: 1550019
34. Kim SK, Hong SR (2014) Gas permeation characteristics of propylene/propane in PEBAX-ZIF composite membranes. Membrane J 24: 259-267
35. Najafi M, Sadeghi M, Shamsabadi Aa, Dinari M, Soroush M (2020) Polysulfone membranes incorporated with reduced graphene oxide nanoparticles for enhanced olefin/paraffin separation. Chemistry Select 5: 3675-3681
36. Shahrezaei K, Abedini R, Lashkarbolooki M, Rahimpour A (2019) A preferential $CO_2$ separation using binary phases membrane consisting of Pebax®1657 and [Omim][PF6] ionic liquid. Korean J Chem Eng 36: 2085-2094
37. Kim M, Kang SW (2019) PEBAX-1657/Ag nanoparticles/7,7,8,8-tetracyanoquinodimethane complex for highly permeable composite membranes with long-term stability. Sci Rep 9: 4266
38. Shao L, Chang X, Zhang Y, Huang Y, Yao Y, Guo Z (2013) Graphene oxide cross-linked chitosan nanocomposite membrane. Appl Surf Sci 280: 989-992
39. Chaiyakun S, Witit-Anun N, Nuntawong N, Chindaudom P, Oaew S, Kedkeaw C, Limsuwan P (2012) Preparation and characterization of graphene oxide nanosheets. Procedia Eng 32: 759-764
40. Meshkat S, Kaliaguine S, Rodrigue D (2019) Enhancing $CO_2$ separation performance of Pebax® MH-1657 with aromatic carboxylic acids. Sep Purif Technol 212: 901-912
41. Khosravi T, Omidkhah M, Kaliaguine S, Rodrigue D (2017) Amine-functionalized CuBTC/poly(ether-b-amide-6) (Pebax® MH 1657) mixed matrix membranes for $CO_2/CH_4$ separation. Can J Chem Eng 95: 2024-2033
42. Farivar F, Lay Yap P, Karunagaran RU, Losic D (2021) Thermogravimetric analysis (TGA) of graphene materials: Effect of particle size of graphene, graphene oxide and graphite on thermal parameters. C 7: 41
43. Losic D, Farivar F, Yap PL, Karami A (2021) Accounting carbonaceous counterfeits in graphene materials using the thermogravimetric analysis (TGA) approach. Anal Chem 93: 11859-11867
44. Nobakht D, Abedini R (2022) Improved gas separation performance of Pebax®1657 membrane modified by poly-alcoholic compounds. J Environ Chem Eng 10: 107568
45. Ranjbar F, Ghorbani M, Abedini R, Ghasemi M (2022) Thin film nanocomposite (TFN) membrane comprising Pebax® 1657 and porous organic polymers (POP) for favored $CO_2$ separation. J Membrane Sci Res 8: 535579
46. Chng ML, Xiao Y, Chung T, Toriida M, Tamai S (2009) Enhanced propylene/propane separation by carbonaceous membrane derived from poly (aryl ether ketone)/2,6-bis(4-azidobenzylidene)-4-methyl-cyclohexanone interpenetrating network. Carbon 47: 1857-1866